Sodium MRI of the human heart at 7.0 T: preliminary results

Graessl, A., Ruehle, A., Waiczies, H., Resetar, A., Hoffmann, S.H., Rieger, J., Wetterling, F., Winter, L., Nagel, A.M., Niendorf, T.

Graessl, A., Ruehle, A., Waiczies, H., Resetar, A., Hoffmann, S. H., Rieger, J., Wetterling, F., Winter, L., Nagel, A. M., and Niendorf, T. (2015) Sodium MRI of the human heart at 7.0 T: preliminary results. NMR Biomed., 28: 967–975. doi: 10.1002/nbm.3338

which has been published in final form in:

NMR in Biomedicine
2015 AUG; 28(8): 967-975
Version of record online: 2015 JUN 17
doi: 10.1002/nbm.3338
Publisher: Wiley-Blackwell

Sodium Magnetic Resonance Imaging of the Human Heart at 7.0 T: Preliminary Results

Andreas Graessl [1], Anjuli Ruehle [1], Helmar Waiczies [3], Ana Resetar[2], Stefan H. Hoffmann [2], Jan Rieger [3], Friedrich Wetterling [4], Lukas Winter [1], Armin M. Nagel [2] and Thoralf Niendorf [1,5]

[1] Berlin Ultrahigh Field Facility (B.U.F.F.), Max-Delbrueck-Center for Molecular Medicine, Berlin, Germany

[2] Division of Medical Physics in Radiology, German Cancer Research Center (DKFZ), Heidelberg, Germany

[3] MRI.TOOLS GmbH, Berlin, Germany

[4] Trinity College, Institute of Neuroscience, The University of Dublin, Ireland

[5] Experimental and Clinical Research Center, A joint cooperation between the Charité Medical Faculty and the Max-Delbrück Center for Molecular Medicine, Berlin, Germany

Corresponding Author: Prof. Dr. Thoralf Niendorf
Berlin Ultrahigh Field Facility (B.U.F.F.)
Max-Delbrueck-Center for Molecular Medicine
Robert-Roessle-Strasse 10
13125 Berlin
Germany
Tel.: +49 30 9406 4505
Fax.: +49 30 9406 49178
E-Mail: Thoralf.Niendorf@mdc-berlin.de

Short Title:

Sodium MR of the Heart at 7.0T

Grant sponsors:

This work was funded in part (A. Graessl, Armin M. Nagel, T. Niendorf) by the Helmholtz Alliance ICEMED – Imaging and Curing Environmental Metabolic Diseases, through the Initiative and Network Fund of the Helmholtz Association. H. Waiczies and L. Winter were funded by the German Federal Ministry of Education and Research ("KMU-innovativ: Medizintechnik MED-373-046).

Word count: 4301
Figures: 5
Tables: 0

Abstract

Objective: Examine the feasibility of three-dimensional and whole heart coverage ^{23}Na cardiac MRI at 7.0 T including single cardiac phase and CINE regimes.

Methods: A four channel transceiver RF coil array tailored for ^{23}Na MRI of the heart at 7.0 T (f=78.5 MHz) is proposed. An integrated bow tie antenna building block is used for ^{1}H MR to support shimming, localization and planning in a clinical workflow. Signal absorption rate simulations and assessment of RF power deposition were performed to meet the RF safety requirements. ^{23}Na cardiac MR was conducted in an in vivo feasibility study. 3D gradient echo (GRE) imaging in conjunction with Cartesian phase encoding (total acquisition time T_{AQ}=6:16 min) and whole heart coverage imaging employing a density-adapted 3D radial acquisition technique (T_{AQ}=18:20 min) were used.

Results: For 3D GRE based ^{23}Na MRI, acquisition of standard views of the heart using a nominal in-plane resolution of (0.5 x 0.5) mm^2 and a slice thickness of 15 mm were feasible. For whole heart coverage 3D density-adapted radial ^{23}Na acquisitions a nominal isotropic spatial resolution of 6 mm was accomplished. This improvement versus 3D conventional GRE acquisitions reduced partial volume effects along the slice direction and enabled retrospective image reconstruction of standard or arbitrary views of the heart. Sodium CINE imaging capabilities were achieved with the proposed RF coil configuration in conjunction with 3D radial acquisitions and cardiac gating. Cardiac gated reconstruction provided an enhancement in blood-myocardium contrast of 20% versus the same data being reconstructed without cardiac gating.

Conclusions: The proposed transceiver array enables ^{23}Na MR of the human heart at 7.0 T within clinical acceptable scan times. This capability is in positive alignment with the needs of explorations that are designed to examine the potential of ^{23}Na MRI for the assessment of cardiovascular and metabolic diseases.

Keywords:
magnetic resonance imaging; ultrahigh field MR; cardiovascular MRI; sodium imaging; RF coil technology; transceiver array

List of Abbreviations

^{23}Na MRI	sodium magnetic resonance imaging
B_0	main magnetic field strengths
B_1^+	electromagnetic transmission field
BMI	body mass index
CP	circular polarized
CNR	contrast-to-noise ratio
ECG	electrocardiogram
Na^+/K^+ ATPase	sodium-potassium adenosine triphosphatase
EMF	electromagnetic fields
f	frequency in Hertz
FA	flip angle in degree
FLASH	Fast Low Angle Shot
FOV	field of view
FR4	copper clad sheet for electronic applications using glass-epoxy resin
IEC	International Electrical Commission
NA	number of averages
NEMA	National Electrical Manufacturers Association
Q_{un}	unloaded quality factor
Q_l	loaded quality factor
RF	radio frequency
RX	reception
S	scattering parameter
SAR	specific absorption rate
SAR_{10g}	specific absorption rate averaged over 10 g
SD	standard deviation
SNR	signal-to-noise ratio
T_1	longitudinal relaxation time
T_2*	effective transversal relaxation time
TE	echo time
TR	repetition time
TX	transmission
UHF-MR	ultrahigh field magnetic resonance

Graphical Abstract (Title, Authors, 80 Words + 5x6cm figure)

Sodium Magnetic Resonance Imaging of the Human Heart at 7.0 T: Preliminary Results

Andreas Graessl, Anjuli Ruehle, Stefan Hoffmann, Helmar Waiczies, Ana Resetar, Jan Rieger, Friedrich Wetterling, Lukas Winter, Armin M. Nagel and Thoralf Niendorf

This pilot study demonstrated the feasibility of sodium MRI of the human heart at 7.0T using a dedicated transceiver RF coil array. The proposed setup afforded the acquisition of sodium images with reasonable myocardial signal in clinically acceptable scan times. 3D density adapted radial acquisitions yielded a signal gain compared to Cartesian gradient echo acquisitions. This improvement supported whole heart, CINE sodium imaging of the heart with an isotropic spatial resolution of 6 mm within approximately 19 minutes scan time.

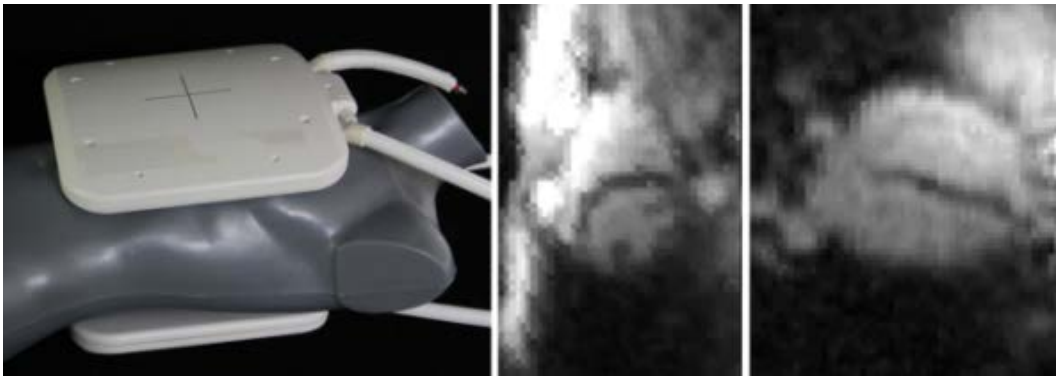

Introduction

Knowledge about compromised cell integrity of myocardial tissue provides valuable information for the assessment of myocardial viability, with tissue sodium concentration being a potent indicator of impaired cellular ion homeostasis and cell membrane integrity. In healthy tissue the Na^+/K^+ATP-ase maintains a transmembrane concentration gradient with an intracellular sodium concentration of about 15 mmol/L against an extracellular concentration of about 140 mmol/L (1,2). During ischemia, for instance, the function of the sodium/potassium pump is compromised by declining energy reserves resulting in increased intracellular sodium concentration.

Sodium MRI (^{23}Na MRI) is a viable approach for gaining better insights into cellular metabolism with a broad spectrum of biomedical imaging research applications (3). Previous studies eloquently reported credible data on ^{23}Na MRI of the heart and demonstrated that ^{23}Na-MRI is suitable for the detection and assessment of acute and chronic heart disease due to increased sodium concentration after myocardial infarction (4-9). These pioneering explorations were primarily limited to animal studies. Constraints dictated by the rapidly decaying ^{23}Na signal and the low sensitivity of ^{23}Na MRI versus clinical ^{1}H-MRI induced scan times being not clinically acceptable and hence constituted a challenge for ^{23}Na MRI of the human heart. Notwithstanding this obstacle ECG gated ^{23}Na MRI of the heart was accomplished for magnetic field strengths commonly used in today's clinical practice ($B_0 \leq 3.0$ T) (10-14). Yet, the low gyromagnetic ratio of ^{23}Na and the low Na^+ tissue concentrations compared with hydrogen resulted in long acquisition times and modest spatial resolution for ^{23}Na MRI

of the heart. Although ample signal-to-noise was demonstrated for ventricular blood, the limited myocardial ^{23}Na signal constitutes a challenge for cardiac sodium MRI *en route* to a clinical tool. Recognizing the sensitivity gain intrinsic to ultrahigh magnetic fields ($B_0 \geq 7.0$ Tesla) and yet unimpaired transmission field homogeneity (15) due to the comparably low ^{23}Na resonance frequency which is close to ^{1}H MRI at 1.5 T it is conceptually appealing to pursue cardiac ^{23}Na-MRI at 7.0 Tesla.

Realizing the challenges of human ^{23}Na MRI alongside the opportunities of ultrahigh field MR (UHF-MR), this study examines the feasibility of cardiac ^{23}Na MRI at clinically acceptable acquisition times using free breathing 3D Cartesian gradient echo and cardiac gated 3D density-adapted radial acquisition techniques at 7.0 T. To meet this goal a local four-element transceiver RF surface coil that is customized for cardiac ^{23}Na MRI at 7.0 T is proposed. To meet the safety and RF power deposition limit requirements of MRI, electromagnetic field (EMF) simulations and specific absorption rate (SAR) considerations are conducted. The feasibility and applicability of the proposed approach for ^{23}Na MRI of the heart at 7.0 T is presented and its suitability for single cardiac phase and for cinematic ^{23}Na MRI is demonstrated in initial volunteer studies, as a precursor to broader clinical studies. The merits and limitations of the proposed transceiver surface coil are discussed and implications for clinical MRI of the human heart at 7.0 T are considered.

Experimental

RF coil design

The proposed dual-frequency RF coil setup (Figure 1a) consists of separate elements for ^{23}Na and ^{1}H MR. For ^{23}Na MR a four channel RF coil array was constructed using two modestly curved lightweight formers to conform to an average anterior and superior chest as illustrated in Figure 1a. Each section contains two rectangular loop elements (size: (210 x 140) mm²) which each share a common conductor as shown in Figure 1b, c. The structure shown in Figure 1b was etched from 32 µm copper on 1 mm FR4 substrate. The conductor thickness was chosen to be more than four times the skin depth of 7.45 µm for copper at 78.6 MHz. Each loop element is divided into five sections by chip capacitors to form a uniform and balanced current distribution along the loop. Distributing the overall capacitance also reduces the voltage at every capacitor and thus reduces coupling to the sample as well as local SAR. A trimmer capacitor (C4) was integrated in the shared conductor to afford adjustable decoupling of the neighboring loop elements (16). The common conductor of the anterior coil section also includes a parallel resonant trap circuit (C6/L6) tuned to 297 MHz to prevent ^{1}H signals to couple into the loop structure. The ports were connected to the coaxial RF feeding cables with a tune/match network consisting of a parallel tuning capacitor and a serial matching trimmer capacitor for each loop element. The coil was tuned to 78.6 MHz which corresponds to the resonance frequency of ^{23}Na at 7.0 T and matched to 50 Ω. Unbalanced currents on the coaxial cables were suppressed by

parallel resonant cable traps. Cable traps were designed as double-turn solenoids of the coaxial cable with an appropriate capacitor soldered to the outer conductor at the crossing of the cable.

Basic ^{1}H imaging capabilities were achieved by a dipole bow tie element tuned to 297 MHz (Figure 1d) as described in (17). The dipole bow tie element was placed inside the left loop element of the anterior section of the ^{23}Na coil as depicted in Figure1 b. This approach provides basic means for localization, B_0 shimming and slice positioning based on ^{1}H images.

Bench measurements and characterization of the RF coil performance were performed using an 8-channel vector network analyzer (ZVT 8, Rohde & Schwarz, Memmingen, Germany). The quality factor ratio Q_U/Q_L of the loop elements was determined based on the measured resonance bandwidth with the array placed on an exemplary human subject. A high value indicates a predominant impact of sample noise over coil noise, which is a key requirement for the applicability of RF coil arrays.

MR hardware

MR experiments were conducted on a 7.0 T whole body MR scanner (Magnetom, Siemens Healthcare, Erlangen, Germany), equipped with an gradient system that offers a maximum slew rate of 200 mT/m/ms and a maximum gradient strength of 40 mT/m (Siemens Medical Solutions, Erlangen, Germany).

An 8 kW single channel RF amplifier was used for ^{1}H MR. An 8 kW broadband single channel x-nuclei RF amplifier (Dressler HF-Technik GmbH, Germany) was used for ^{23}Na MR. The x-nuclei amplifier output was split into 4 equal-amplitude signals by

means of three hybrid couplers (Anaren Microwave Inc., New York, US) compiled to a splitting cascade from 1:2 and 2:4. Phase adjustments of the single channels were implemented by phase-shifting coaxial cables connected to the power splitting network. The four ^{23}Na elements and the one ^{1}H element were connected to the RF system using an interface box with transmit/receive switches and integrated low-noise preamplifiers designed for the corresponding frequencies (Stark Contrast, Erlangen, Germany).

Electromagnetic field simulations

EMF and SAR simulations were performed using the finite integration technique of CST Studio Suite 2012 (CST AG, Darmstadt, Germany) together with human voxel model Duke (BMI: 23.1) (18). The simulations included the RF shield of the gradient coil. The voxel model was truncated at the neck and at the hips as displayed in Figure 1e, allowing for a high resolution mesh in the target region formed around the heart. Two simulations were performed with voxel model tissue parameters corresponding to 78.6 MHz and 297 MHz as listed in (19) to estimate SAR values for the respective frequencies. Decoupling capacitors and the feeding points of the elements were modeled as 50 Ω ports. Final field results were accomplished incorporating lumped decoupling, tuning and matching capacitors in the built-in circuit simulator of CST Studio Suite (CST Design Studio 2012), following the circuit co-simulation workflow proposed in (20). The capacitor values were optimized with respect to the S-parameter simulation and were used as a starting point for the practical realization. For the final configuration and phase settings used in in vivo measurements SAR values were calculated. The input power was adjusted to meet the regulations of the IEC guideline IEC 60601-2-33

Ed.3 (21). At 78.6 MHz, which is in the frequency range of 1.5T proton imaging, transmission field non-uniformities are expected to present no major practical obstacle for ^{23}Na MRI at 7.0 T. A circular polarized (CP) like mode is used for transmission. The CP mode refers to a phase setting with each channel driven by a phase corresponding to its angular position relative to the body center in the transversal plane (Channel1: 0°, channel2: -305°, channel3: -136°, channel4: -93°).

Ethics statement

For the in vivo feasibility study, subjects without any known history of cardiac disease were included after due approval by the local ethical committee (registration number DE/CA73/5550/09, Landesamt für Arbeitsschutz, Gesundheitsschutz und technische Sicherheit, Berlin, Germany). Informed written consent was obtained from each volunteer prior to the study.

Cardiac imaging protocol

In vivo cardiac MR was performed in three healthy subjects (2 male, 1 female; age range: 26 - 29; BMI range: 19 - 22, heart rate range: 62 - 78 bpm).

^{1}H imaging was performed using 2D CINE FLASH imaging (matrix size 256x256, TE=1.84 ms, TR=4.14 ms, voxel size (1.4x1.4x4.0) mm³, number of cardiac phases=30, total acquisition time= 0:16 min). For cardiac imaging slice positioning was carried out following international consensus (22,23). For this purpose the heart was localised in three orthogonal thoracic slices placed along each main axis of the upper torso using

single breath-hold, low spatial resolution 2D gradient echo scout images. The long axis of the left ventricle was dissected twice, and finally a stack of short axes was obtained. These slices provided the basis for planning standard long axis views (four-chamber, three-chamber and two-chamber view) derived from 2D CINE FLASH imaging. Based on the four-chamber view, a mid-ventricular short axes view positioned parallel to the mitral valve plane was planned. The obtained slice positions were subsequently used for slab and 3D volume positioning for ^{23}Na imaging.

For ^{23}Na MRI of the heart flip angle calibration was done offline (Matlab, Mathworks, Natick, USA) using a curve fitting algorithm on a set of signal intensity points which were acquired with a series of RF transmitter reference amplitudes. For flip angle calibration the whole field of view was taken into account. ^{23}Na MRI of the heart was performed with two imaging protocols:

- short axis views and four chamber views of the heart were acquired using untriggered, free breathing 3D gradient echo (3D FLASH) imaging with Cartesian phase encoding: matrix size 64 x 48, echo time TE=1.91 ms, repetition time TR=28 ms, voxel size (5 x 5 x 15) mm³, number of averages 35, receiver bandwidth=120 Hz/pixel, flip angle= 28°, 8 slices per slab, total acquisition time 6:16 min.
- whole heart coverage ^{23}Na datasets were acquired with a density-adapted 3D radial acquisition technique (24): TE= 0.4 ms, TR=11 ms, T_{RO}= 7.1 ms, flip angle= 36°, number of projections=10000, number of averages=10, voxel size=(6 x 6 x 6 mm)³, total acquisition time=18:20 min.

For ^{1}H and ^{23}Na MRI of the heart synchronization of the data acquisition with the cardiac cycle was achieved using an acoustic cardiac gating device using an MR compatible stethoscope (easyACT, MRI.Tools GmbH, Berlin, Germany) (25-28).

Data reconstruction and image analysis

For 3D radial ^{23}Na acquisitions the slice positioning given by the ^{1}H images was used to extract the standard cardiac views from the reconstructed 3D dataset. Three reconstruction modi were applied for the 3D datasets obtained with the density-adapted 3D radial acquisition technique:

- ungated reconstruction of the acquired data
- retrospectively gated reconstruction using a temporal resolution of 0.1 s and time increments of 0.05 s. With this approach ^{23}Na CINE images with 20 frames per cardiac cycle were reconstructed from the 3D acquisitions.
- retrospectively gated and cardiac phase selective reconstruction for data acquired during diastole. Based on the trigger information data acquired during systole were discarded.

Signal-to-noise ratio (SNR) maps were estimated using method 4 proposed in the NEMA standard MS-1 (29). According to (29) the noise in magnitude images is given by the standard deviation of the signal in a noise-only region divided by the factor 0.66. To eliminate the impact of potential artifacts of the radial acquisition scheme in any region of the image, the standard deviation of noise was derived from a separate noise scan. Contrast-to-noise-ratio (CNR) values were estimated by subtraction of the mean SNR value inside myocardium from the mean SNR of the left ventricular blood

pool. To examine the SNR profile along a circular trajectory inside the myocardium mid-ventricular short axis SNR maps were analyzed. For this purpose a standardized myocardial segmentation and nomenclature for tomographic imaging of the heart was used (30).

Results

Hardware and RF characteristics

The loaded (Q_L) and unloaded quality factor (Q_U) were obtained by loading and unloading the RF coil on a subject. The ^{23}Na loop elements provided an average Q_L/Q_U ratio of 0.12, indicating the dominance of sample noise. Reflection coefficients of -15 dB or less were observed. Element coupling was below -20 dB for the neighboring elements. Anterior posterior coupling was below noise level. The reflection coefficient of the ^{1}H dipole was -26 dB. The decoupling of the ^{23}Na loop elements to the ^{1}H dipole was below -49 dB at 78.6 MHz and below -26 dB at 297 MHz for all ^{23}Na loop elements. The complete set of S-parameters for both frequencies is surveyed in Figure 2 a, b.

Overall losses from the systems RF output to the individual coil connectors were determined to be -0.7 dB for the ^{23}Na RF chain and –1.4 dB for the ^{1}H path, which were considered for the RF input power settings.

EMF and SAR Simulations

Figure 2c shows the combined transmit field for the ^{23}Na array driven with the CP like phase setting for a transversal slice through the human voxel model's heart. SAR_{10g} values derived from the EMF simulations are outlined in Figure 2d. For the CP like mode the maximum local SAR_{10g} per input power was found to be 0.39 1/kg. For the ^{1}H dipole element the transmit field is shown in Figure 2e. The local SAR_{10g} assessment yielded a local SAR_{10g} per input power of 1.46 1/kg. With an input power of 25 W_{RMS} for

the ^{23}Na array and 6.8 W_{RMS} input power for the ^{1}H dipole and with considering the measured power losses in the RF chain, SAR_{10g} values were below the limits permitted by the IEC guidelines (21). The first and second level controlled mode given by the IEC guidelines were not used for in vivo imaging which limits the maximum local SAR_{10g} to 10 W/kg and preserves a safety margin of factor 2.

Cardiac MR imaging

The integrated dipole element supported basic ^{1}H MR for localization as illustrated in Figure 3a. This enabled shimming planning of standard cardiac views in a clinical workflow for subsequent ^{23}Na imaging. For ^{23}Na MRI the transmitter reference amplitude was found to be 680±11 V, leading to a 180° pulse with a rectangular pulse applied for 1 ms.

For 3D gradient echo based ^{23}Na MRI of the heart a nominal in-plane resolution of (5 x 5) mm² and a slice thickness of 15 mm was found to be feasible. Figure 3b depicts a short axis view of the heart derived from 3D gradient echo based imaging. The cardiac SNR evaluated over all volunteers was found to be 15±4 in the blood pool and 10±3 in the myocardium. A detailed SNR evaluation along the myocardial segments of a mid-ventricular short axis view is outlined in Figure 3c. A blood myocardium contrast of 4 was obtained. A high signal intensity caused by the high ^{23}Na concentration of rib cartilage was observed (Figure 3b).

For whole heart coverage 3D density-adapted radial ^{23}Na acquisitions a nominal spatial resolution of 6 mm isotropic was achieved. This improvement versus 3D conventional gradient echo acquisitions helped to reduce partial volume effects along

the slice direction and enabled retrospective image reconstruction of standard or arbitrary views of the heart. Figure 4a shows a whole heart coverage short axis view of the heart reconstructed from 3D radial acquisitions without using cardiac gating. A stack of short axis views covering the heart form the apex to the base shows consistent image quality for all slices reconstructed. Averaged over all subjects, mid-ventricular short axis views (Figure 4b) exhibited a SNR of 38±4 for the blood pool while myocardium revealed an SNR of 25±4. This provided a mean blood/ myocardium contrast of 13. An exemplary SNR evaluation along the myocardial segments of a mid-ventricular short axis view shown in Figure 4b is illustrated in Figure 4c. In companion, a four chamber view of the heart reconstructed from the same 3D data set is shown in Figure 4d.

Figure 5 illustrates the sodium CINE imaging capabilities achieved with the proposed RF coil configuration in conjunction with 3D radial acquisitions and cardiac gating. Figure 5 a,b show end-systolic and end-diastolic short axis views of the heart derived from a CINE dataset consisting of 20 cardiac phases. To illustrate the movement and contrast throughout the cardiac cycle, a signal intensity profile along the long axis of the heart was extracted for every cardiac phase and summarized in the M-mode like view shown in Figure 5c.

Figure 5 d-e illustrates the impact of cardiac gating on the delineation of the myocardium. Figure 5d shows an un-triggered reconstruction. Figure 5e depicts the result of a cardiac gated reconstruction, based on data acquired during diastole only. The difference map in Figure 5f reveals a higher signal for the cardiac gated reconstruction inside the blood pool for regions in proximity to the myocardium. This

results in a blood-myocardium contrast enhancement of 20% versus the same data being reconstructed without cardiac gating.

Discussion

This feasibility study adds to the literature by demonstrating the feasibility of ^{23}Na MRI of the human heart at 7.0 T. The evidence herein suggests that ^{23}Na MRI at 7.0 T provides sensitivity and spatiotemporal resolution advantages over studies at 1.5 T and 3.0 T (10-12). The proposed RF coil setup exhibits adequate RF characteristics, transmission field homogeneity and penetration depth that support sodium imaging of the heart at 7.0 T in clinically acceptable scan times including free breathing, cardiac gated and ungated acquisitions. Depending on the acquisition technique used the SNR of myocardium was found to be between 10 and 27 for mid-ventricular short axis views of the heart. This achievement supports clear delineation of the myocardium including deep lying regions of the heart. The latter was reported to constitute a challenge for ^{23}Na MR at a field strength of 3.0 T (31). Our in vivo studies in healthy subjects revealed that the use of a density-adapted 3D radial acquisition protocol used here provides an SNR advantage of roughly 80% compared to the used 3D gradient echo protocol. Pointing out this large gain we anticipate that differences in the calculation of the spatial resolution between Cartesian and radial acquisition protocols might slightly alter this value. The signal gain is related to the different echo times feasible for the 3D radial acquisition and the 3D gradient echo protocol due to the fast transverse relaxation of the sodium signal. Assuming a rapidly decaying component with $T_{2,rapid}$*=(0.5-4.0) ms and a slowly decaying component with $T_{2,low}$*=(12-20) ms (14), an SNR gain of 27% to 85% can be expected when TE is reduced from 1.9 ms to 0.4 ms. Additionally, different

pulse sequence parameters (e.g. TR) might contribute to the SNR gain. Yet, the sensitivity gain of the density-adapted 3D radial acquisition protocol enabled sodium CINE imaging of the heart with 10 frames per cardiac cycle within an acquisition time of approximately 19 min. Cardiac triggering can be considered being beneficial to enhance the delineation of myocardium and the blood pool for a diastolic cardiac phase, since the epi- and endocardial boarder sharpness was improved by not including data acquired during cardiac phases of myocardial contraction and relaxation. The 6 mm isotropic resolution of the whole heart 3D radial acquisitions facilitated the reconstruction of arbitrary cardiac views including a stack of short axis and four chamber standard cardiac views from a single acquisition.

Efficient and uniform RF excitation of the upper torso might present a challenge. This can be accomplished with a whole body RF coil as recently reported for ^{23}Na MR at 3.0 T using a 16-rung birdcage resonator body coil (32). Since available transmit RF power is limited the high transmit power requirements of volume coils constrain the flip angles needed for short excitation pulses used in sodium MRI. The higher efficiency of a local transceiver array proposed in this work offsets this constraint since the applicable flip angles are restricted by SAR limitations rather than by RF peak power constraints. To our knowledge, this is the first cardiac ^{23}Na MR study conducted with a multi-element transceiver coil.

The preliminary results reported for this feasibility study are likely to pave the way for further advances in RF coil technology tailored for assessment of myocardial sodium content. These efforts will help to further gain sensitivity by reducing loop element size and by including more loop elements and hence will contribute to further improvements

in spatio-temporal resolution. For example a two channel transmit loop together with a 8 channel receive array was reported to be feasible for sodium cardiac imaging at 3.0 T (33). The measured Q-ratio of 8 for the proposed four channel transceiver array leaves reasonable space for further subdivision of the elements into an array of eight or more TX/RX elements as recently demonstrated for transceiver arrays customized for ^{1}H MRI at 7.0 T (34-41), To advance the proton imaging capabilities it stands to reason to incorporate multiple ^{1}H elements into the anterior and posterior sections of the ^{23}Na array to support high spatial resolution and accelerated imaging of the heart (42-48). This can either be achieved by dipole elements placed inside the loops or by overlapping loops for proton imaging as reported previously for a lower abdomen RF coil (49). For this purpose the bowtie radiative elements used here can be replaced by other dipole configurations including loopoles or bended dipoles (50,51).

We recognized limitations in our feasibility study, which included healthy volunteers before extra variances due to pathophysiological conditions are introduced. Taking into account that cardiac MR at 7.0 T is a field in a state of creative flux we felt that it is important to begin by reporting on the details of our preliminary results deduced from ^{23}Na MRI of the heart before the technology will be placed in the hands of a broader group of clinical colleagues. Because of the physiological relevance of the intra- versus the extracellular sodium compartment, a separation between these pools constitutes another goal for the development of ^{23}Na-MRI techniques employing relaxation-weighted imaging, multiple-quantum filtering (52-56) or bi-exponential-weighted imaging (57,58). Explorations into appropriate suppression or selective excitation techniques would be beneficial for suppression of signal contributions from

blood and cartilage which would help to enhance the dynamic range available for myocardial signal. For example, the cartilage signal could be spoiled by using a local surface gradient coil placed around the stenum on top of the chest. We are aware that spill-over effects from signal contributions of the blood pool might still constitute a challenge for myocardial sodium assessment in routine clinical applications of ^{23}Na MRI. In analogy to recent pioneering reports on ^{23}Na MR of the brain iterative reconstruction techniques that consider information from ^{1}H imaging could be utilized to improve spatial resolution for sodium imaging of the heart at 7.0 T (59). Additionally, the blood signal could be eliminated by using inversion-recovery or relaxation-weighted imaging. For quantitative assessment of myocardial tissue sodium concentration, partial volume correction methods might be applied. For this purpose the geometric transfer matrix algorithm might be used (60). This algorithm was designed for positron emission tomography and recently transferred to non-proton MRI (61).

With the preliminary results achieved in this study we anticipate to make use of the proposed RF configuration for driving translational research. While being important but beyond the scope of this work, application of the proposed ^{23}Na MRI setup could benefit the assessment of sodium homeostasis and myocardial viability (2,3,5). Furthermore, ^{23}Na MRI at 7.0 T could provide means for the examination of cardiac sodium channelopathies (62). It is also clinically appealing to pursue sodium MRI of the heart at 7.0 T to gain better insights into hypertrophic cardiomyopathy (HCM). Previous animal studies reported a decrease in Na^{+},K-ATPase activity for HCM, which resulted in a 40% increase in intracellular sodium concentration (63). ^{23}Na MR at 7.0 T could be

also beneficial for scrutinizing alterations in the myocardial Na^+ concentration evoked by cardiac drugs acting upon sodium ion channels (64-66).

Quantification of myocardial sodium concentration requires correction of coil-array sensitivity variation over the heart. This can be accomplished with B_1 mapping to derive the coil array's transmission field distribution and the coil array's sensitivity profile as demonstrated for various RF coil configurations tailored for ^{23}Na or other x-nuclei MRI at 3.0 T and 7.0 T (67-69). Improving in-plane spatial resolution of sodium MRI may be another important aspect to support these clinical applications. While the proposed RF coil design is tailored to the heart it can be adapted to support in vivo assessment of human sodium content in body sections other than the heart including the kidney or skin (67,70).

To conclude, the proposed transceiver array enables sodium imaging of the human heart at 7.0 T within clinical acceptable scan times and provides encouragement for further explorations into densely packed multichannel transceiver coil arrays tailored for ^{23}Na cardiac MR. The benefits of such improvements would be in positive alignment with the needs of explorations that are designed to examine the potential of ^{23}Na MRI for the assessment of myocardial ischemia and cell integrity. We suggest that ^{23}Na CMR at 7.0 T can also help to unlock questions regarding Na^+ balance and Na^+ storage functions of myocardial tissue with the ultimate goal to provide imaging means for diagnostics and for guiding treatment decisions in cardiovascular and metabolic diseases.

Acknowledgements

This work was funded in part (A. Graessl, Armin M. Nagel, T. Niendorf) by the Helmholtz Alliance ICEMED – Imaging and Curing Environmental Metabolic Diseases, through the Initiative and Network Fund of the Helmholtz Association. H. Waiczies and L. Winter were funded by the German Federal Ministry of Education and Research (“KMU-innovativ: Medizintechnik MED-373-046).

References

1. Polimeni PI. Extracellular space and ionic distribution in rat ventricle. Am J Physiol 1974;227(3):676-683.
2. Robinson J. The (Na+ + K+)-activated ATPase Enzymatic and transport properties. Biochimica et Biophysica Acta (BBA) - Reviews on Bioenergetics 1979;549(2):145–176.
3. Madelin G, Regatte RR. Biomedical applications of sodium MRI in vivo. J Magn Reson Imaging 2013;38(3):511-529.
4. Constantinides CD, Kraitchman D, O'Brien K, Boada F, Gillen J, Bottomley PA. Noninvasive quantification of total sodium concentrations in acute reperfused myocardial infarction using 23Na MRI. Magn Reson Med 2001;46(6):1144-1151.
5. Kim RJ, Lima JAC, Chen EL, Reeder SB, Klocke FJ, Zerhouni EA, Judd RM. Fast 23Na magnetic resonance imaging of acute reperfused myocardial infarction: potential to assess myocardial viability. Circulation 1997;95(7):1877.
6. Rochitte CE, Kim RJ, Hillenbrand HB, Chen E, Lima JAC. Microvascular integrity and the time course of myocardial sodium accumulation after acute infarction. Circ Res 2000;87(8):648.
7. Sandstede J, Pabst T, Beer M, Harre K, Bäurle K, Lipke C, Butter F, Kenn W, Völker W, Neubauer S. 23 Natrium-MRT zur Infarktdarstellung am menschlichen Herzen. ROFO 2000;172(9):739-743.
8. Beer M, Sandstede J, Pabst T, Landschütz W, Harre K, Kienlin Mv, Voelker W, Neubauer S, Hahn D. Assessment of myocardial viability by 31P-MR-spectroscopy and 23Na-MR imaging. MAGMA 2000;11(1-2):44–46.
9. Sandstede JJW, Hillenbrand H, Beer M, Pabst T, Butter F, Machann W, Bauer W, Hahn D, Neubauer S. Time course of 23Na signal intensity after myocardial infarction in humans. Magn Reson Med 2004;52(3):545–551.
10. Jerecic R, Bock M, Nielles-Vallespin S, Wacker C, Bauer W, Schad LR. ECG-gated 23Na-MRI of the human heart using a 3D-radial projection technique with ultra-short echo times. MAGMA 2004;16(6):297–302.

11. Konstandin S, Schad LR. Two-dimensional radial sodium heart MRI using variable-rate selective excitation and retrospective electrocardiogram gating with golden angle increments. Magn Reson Med 2013;70(3):791–799.
12. Robson MD, Titus L, Neubauer S. Cardiac sodium imaging with phased arrays at 3 Tesla using a 3D Ultra-short TE (UTE) approach. J Cardiovasc Magn Reson 2008;10(Suppl 1):A109.
13. Ouwerkerk R, Weiss RG, Bottomley PA. Measuring human cardiac tissue sodium concentrations using surface coils, adiabatic excitation, and twisted projection imaging with minimal T2 losses. J Magn Reson Imaging 2005;21(5):546–555.
14. Bottomley PA. Sodium Sodium MRI in human heart: a review. NMR Biomed 2015; DOI: 10.1002/nbm.3265 [epub ahead of print].
15. Niendorf T, Graessl A, Thalhammer C, Dieringer MA, Kraus O, Santoro D, Fuchs K, Hezel F, Waiczies S, Ittermann B, Winter L. Progress and promises of human cardiac magnetic resonance at ultrahigh fields: a physics perspective. J Magn Reson 2013;229:208-222.
16. Roemer PB, Edelstein WA, Hayes CE, Souza SP, Mueller OM. The NMR phased array. Magn Reson Med 1990;16(2):192-225.
17. Winter L, Özerdem C, Hoffmann W, Santoro D, Müller A, Waiczies H, Seemann R, Graessl A, Wust P, Niendorf T, Yacoub E. Design and Evaluation of a Hybrid Radiofrequency Applicator for Magnetic Resonance Imaging and RF Induced Hyperthermia: Electromagnetic Field Simulations up to 14.0 Tesla and Proof-of-Concept at 7.0 Tesla. PLoS ONE 2013;8(4):e61661.
18. Christ A, Kainz W, Hahn EG, Honegger K, Zefferer M, Neufeld E, Rascher W, Janka R, Bautz W, Chen J, Kiefer B, Schmitt P, Hollenbach H-P, Shen J, Oberle M, Szczerba D, Kam A, Guag JW, Kuster N. The Virtual Family--development of surface-based anatomical models of two adults and two children for dosimetric simulations. Phys Med Biol 2010;55(2):N23-38.
19. Gabriel C, Gabriel S. Compilation of the Dielectric Properties of Body Tissues at RF and Microwave Frequencies.
20. Kozlov M, Turner R. Fast MRI coil analysis based on 3-D electromagnetic and RF circuit co-simulation. J Magn Reson 2009;200(1):147–152.

21. Commission IE. Medical electrical equipment. Part 2-33: Particular requirements for the safety of magnetic resonance equipment for medical diagnosis. IEC 60601-2-33. Geneva: IEC.
22. Kramer CM, Barkhausen J, Flamm SD, Kim RJ, Nagel E. Standardized cardiovascular magnetic resonance imaging (CMR) protocols, society for cardiovascular magnetic resonance: board of trustees task force on standardized protocols. J Cardiovasc Magn Reson 2008;10:35.
23. Kramer CM, Barkhausen J, Flamm SD, Kim RJ, Nagel E. Standardized cardiovascular magnetic resonance (CMR) protocols 2013 update. J Cardiovasc Magn Reson 2013;15:91.
24. Nagel AM, Laun FB, Weber M-A, Matthies C, Semmler W, Schad LR. Sodium MRI using a density-adapted 3D radial acquisition technique. Magn Reson Med 2009;62(6):1565–1573.
25. Frauenrath T, Niendorf T, Kob M. Acoustic method for synchronization of Magnetic Resonance Imaging (MRI). Acta Acustica united with Acustica 2008(94):148-155.
26. Frauenrath T, Hezel F, Heinrichs U, Kozerke S, Utting JF, Kob M, Butenweg C, Boesiger P, Niendorf T. Feasibility of cardiac gating free of interference with electro-magnetic fields at 1.5 Tesla, 3.0 Tesla and 7.0 Tesla using an MR-stethoscope. Invest Radiol 2009;44(9):539-547.
27. Becker M, Frauenrath T, Hezel F, Krombach GA, Kremer U, Koppers B, Butenweg C, Goemmel A, Utting JF, Schulz-Menger J, Niendorf T. Comparison of left ventricular function assessment using phonocardiogram- and electrocardiogram-triggered 2D SSFP CINE MR imaging at 1.5 T and 3.0 T. Eur Radiol 2010;20(6):1344-1355.
28. Frauenrath T, Hezel F, Renz W, d'Orth Tde G, Dieringer M, von Knobelsdorff-Brenkenhoff F, Prothmann M, Schulz Menger J, Niendorf T. Acoustic cardiac triggering: a practical solution for synchronization and gating of cardiovascular magnetic resonance at 7 Tesla. J Cardiovasc Magn Reson 2010;12:67.

29. Association NEM. NEMA Standards Publication MS 1-2008 Determination of Signal-to-Noise Ratio (SNR) in Diagnostic Magnetic Resonance Imaging. Rosslyn, VA 22209: National Electrical Manufacturers Association.
30. Cerqueira M, Weissman N, Dilsizian V, Jacobs A, Kaul S, Laskey W, Pennell D, Rumberger J, Ryan T, Verani M. Standardized myocardial segmentation and nomenclature for tomographic imaging of the heart: a statement for healthcare professionals from the Cardiac Imaging Committee of the Council on Clinical Cardiology of the American Heart Association. Circulation 2002;105:539 - 542.
31. Gai ND, Rochitte C, Nacif MS, Bluemke DA. Optimized three-dimensional sodium imaging of the human heart on a clinical 3T scanner. Magn Reson Med 2015;73:623-632.
32. Wetterling F, Corteville DM, Kalayciyan R, Rennings A, Konstandin S, Nagel AM, Stark H, Schad LR. Whole body sodium MRI at 3T using an asymmetric birdcage resonator and short echo time sequence: first images of a male volunteer. Phys Med Biol 2012;57(14):4555–4567.
33. Lanz T, Mayer M, Robson MD, Neubauer S, Ruff J, Weisser A. An 8 Channel 23Na Heart Array for Application at 3 T. In: Ismrm, editor. Proc Intl Soc Mag Reson Med 15; 2007. p 241.
34. Niendorf T, Sodickson DK, Krombach GA, Schulz-Menger J. Toward cardiovascular MRI at 7 T: clinical needs, technical solutions and research promises. Eur Radiol 2010;20(12):2806-2816.
35. Dieringer MA, Renz W, Lindel T, Seifert F, Frauenrath T, von Knobelsdorff-Brenkenhoff F, Waiczies H, Hoffmann W, Rieger J, Pfeiffer H, Ittermann B, Schulz-Menger J, Niendorf T. Design and application of a four-channel transmit/receive surface coil for functional cardiac imaging at 7T. J Magn Reson Imaging 2011;33(3):736-741.
36. Winter L, Kellman P, Renz W, Grassl A, Hezel F, Thalhammer C, von Knobelsdorff-Brenkenhoff F, Tkachenko V, Schulz-Menger J, Niendorf T. Comparison of three multichannel transmit/receive radiofrequency coil configurations for anatomic and functional cardiac MRI at 7.0T: implications for clinical imaging. Eur Radiol 2012;22(10):2211-2220.

37. Thalhammer C, Renz W, Winter L, Hezel F, Rieger J, Pfeiffer H, Graessl A, Seifert F, Hoffmann W, von Knobelsdorff-Brenkenhoff F, Tkachenko V, Schulz-Menger J, Kellman P, Niendorf T. Two-dimensional sixteen channel transmit/receive coil array for cardiac MRI at 7.0 T: design, evaluation, and application. J Magn Reson Imaging 2012;36(4):847-857.
38. Grassl A, Winter L, Thalhammer C, Renz W, Kellman P, Martin C, von Knobelsdorff-Brenkenhoff F, Tkachenko V, Schulz-Menger J, Niendorf T. Design, evaluation and application of an eight channel transmit/receive coil array for cardiac MRI at 7.0 T. Eur J Radiol 2013;82(5):752-759.
39. Graessl A, Muhle M, Schwerter M, Rieger J, Oezerdem C, Santoro D, Lysiak D, Winter L, Hezel F, Waiczies S, Guthoff RF, Falke K, Hosten N, Hadlich S, Krueger PC, Langner S, Stachs O, Niendorf T. Ophthalmic magnetic resonance imaging at 7 T using a 6-channel transceiver radiofrequency coil array in healthy subjects and patients with intraocular masses. Invest Radiol 2014;49(5):260-270.
40. Graessl A, Renz W, Hezel F, Dieringer MA, Winter L, Oezerdem C, Rieger J, Kellman P, Santoro D, Lindel TD, Frauenrath T, Pfeiffer H, Niendorf T. Modular 32-channel transceiver coil array for cardiac MRI at 7.0T. Magn Reson Med 2014;72(1):276-290.
41. Niendorf T, Paul K, Oezerdem C, Graessl A, Klix S, Huelnhagen T, Hezel F, Rieger J, Waiczies H, Frahm J, Nagel A, Oberacker E, Winter L. W(h)ither Human Cardiac and Body Magnetic Resonance at Ultrahigh Fields? Technical Advances, Practical Considerations, Applications, and Clinical Opportunities NMR Biomed 2015; DOI: 10.1002/nbm.3268 [epub ahead of publication].
42. von Knobelsdorff-Brenkenhoff F, Frauenrath T, Prothmann M, Dieringer MA, Hezel F, Renz W, Kretschel K, Niendorf T, Schulz-Menger J. Cardiac chamber quantification using magnetic resonance imaging at 7 Tesla--a pilot study. Eur Radiol 2010;20(12):2844-2852.
43. Hezel F, Thalhammer C, Waiczies S, Schulz-Menger J, Niendorf T. High spatial resolution and temporally resolved T2* mapping of normal human myocardium at 7.0 Tesla: an ultrahigh field magnetic resonance feasibility study. PLoS One 2012;7(12):e52324.

44. von Knobelsdorff-Brenkenhoff F, Tkachenko V, Winter L, Rieger J, Thalhammer C, Hezel F, Graessl A, Dieringer MA, Niendorf T, Schulz-Menger J. Assessment of the right ventricle with cardiovascular magnetic resonance at 7 Tesla. J Cardiovasc Magn Reson 2013;15:23.
45. Niendorf T, Sodickson DK. Highly accelerated cardiovascular MR imaging using many channel technology: concepts and clinical applications. Eur Radiol 2008;18(1):87-102.
46. Niendorf T, Sodickson DK. Parallel imaging in cardiovascular MRI: methods and applications. NMR Biomed 2006;19(3):325-341.
47. Niendorf T, Sodickson D. [Acceleration of cardiovascular MRI using parallel imaging: basic principles, practical considerations, clinical applications and future directions]. Rofo 2006;178(1):15-30.
48. Niendorf T, Hardy CJ, Giaquinto RO, Gross P, Cline HE, Zhu Y, Kenwood G, Cohen S, Grant AK, Joshi S, Rofsky NM, Sodickson DK. Toward single breath-hold whole-heart coverage coronary MRA using highly accelerated parallel imaging with a 32-channel MR system. Magn Reson Med 2006;56(1):167-176.
49. Bae KT, Kim J-H, Furlan A, Moon C, Park B, Zhao T. Proton and sodium MR imaging of in vivo human prostate using dual-tuned body and endorectal coils at 7T. In: Ismrm, editor. Proc Intl Soc Mag Reson Med 18; 2010. p 2693.
50. Lakshmanan K, Cloos M, Lattanzi R, Sodickson DK, Wiggins GC. The Loopole Antenna: Capturing Magnetic and Electric Dipole Fields with a Single Structure to Improve Transmit and Receive Performance. In: Ismrm, editor. Proc Intl Soc Mag Reson Med 22; 2014. p 397.
51. Chen G, Cloos M, Lattanzi R, Sodickson DK, Wiggins GC. Bent Electric Dipoles: A Novel Coil Design Inspired by the Ideal Current Pattern for Central SNR at 7 Tesla. In: Ismrm, editor. Proc Intl Soc Mag Reson Med 22; 2014. p 402.
52. Fiege DP, Romanzetti S, Mirkes CC, Brenner D, Shah NJ. Simultaneous single-quantum and triple-quantum-filtered MRI of 23Na (SISTINA). Magn Reson Med 2013;69(6):1691-1696.
53. Konstandin S, Nagel AM. Measurement techniques for magnetic resonance imaging of fast relaxing nuclei. MAGMA 2014;27(1):5-19.

54. Nagel AM, Amarteifio E, Lehmann-Horn F, Jurkat-Rott K, Semmler W, Schad LR, Weber M-A. 3 Tesla sodium inversion recovery magnetic resonance imaging allows for improved visualization of intracellular sodium content changes in muscular channelopathies. Invest Radiol 2011;46(12):759–766.
55. Pekar J, Leigh JS. Detection of biexponential relaxation in sodium-23 facilitated by double-quantum filtering. J Magn Reson 1986;69(3):582–584.
56. Jaccard G, Wimperis S, Bodenhausen G. Multiple-quantum NMR spectroscopy of S=3/2 spins in isotropic phase: A new probe for multiexponential relaxation. J Chem Phys 1986;85(11):6282.
57. Benkhedah N, Bachert P, Semmler W, Nagel AM. Three-dimensional biexponential weighted (23) Na imaging of the human brain with higher SNR and shorter acquisition time. Magn Reson Med 2012.
58. Benkhedah N, Bachert P, Nagel AM. Two-pulse biexponential-weighted 23Na imaging. J Magn Reson 2014;240:67–76.
59. Gnahm C, Nagel AM. Anatomically weighted second-order total variation reconstruction of 23Na MRI using prior information from 1H MRI. Neuroimage 2015;105:452-461.
60. Rousset OG, Ma Y, Evans AC. Correction for partial volume effects in PET: principle and validation. J Nucl Med 1998;39(5):904-911.
61. Hoffmann SH, Radbruch A, Bock M, Semmler W, Nagel AM. Direct (17)O MRI with partial volume correction: first experiences in a glioblastoma patient. MAGMA 2014;27(6):579-587.
62. Amin AS, Asghari-Roodsari A, Tan HL. Cardiac sodium channelopathies. Pflugers Arch 2010;460(2):223-237.
63. Norgaard A, Baandrup U, Larsen JS, Kjeldsen K. Heart Na,K-ATPase activity in cardiomyopathic hamsters as estimated from K-dependent 3-O-MFPase activity in crude homogenates. J Mol Cell Cardiol 1987;19(6):589-594.
64. Fredj S, Sampson KJ, Liu H, Kass RS. Molecular basis of ranolazine block of LQT-3 mutant sodium channels: evidence for site of action. Br J Pharmacol 2006;148(1):16-24.

65. Duff HJ, Cannon NJ, Sheldon RS. Mexiletine-quinidine in isolated hearts: an interaction involving the sodium channel. Cardiovasc Res 1989;23(7):584-592.
66. Sheldon RS, Hill RJ, Duff HJ. Antiarrhythmic drugs and the cardiac sodium channel: current models. Clin Chem 1989;35(5):748-754.
67. Linz P, Santoro D, Renz W, Rieger J, Ruehle A, Ruff J, Deimling M, Rakova N, Muller DN, Luft FC, Titze J, Niendorf T. Skin sodium measured with (23) Na MRI at 7.0 T. NMR Biomed 2015;28(1):54-62.
68. Kopp C, Linz P, Wachsmuth L, Dahlmann A, Horbach T, Schofl C, Renz W, Santoro D, Niendorf T, Muller DN, Neininger M, Cavallaro A, Eckardt KU, Schmieder RE, Luft FC, Uder M, Titze J. (23)Na magnetic resonance imaging of tissue sodium. Hypertension 2012;59(1):167-172.
69. Yiyi J, Waiczies H, Winter L, Neumanova P, Hoffmann D, Rieger J, Mekle R, Waiczies H, Niendorf T. Eight channel transceiver radiofrequency coil array tailored for 1H/19F magnetic resonance of the human knee and fluorinated drugs at 7.0 Tesla. NMR Biomed; in press 2015.
70. Haneder S, Juras V, Michaely HJ, Deligianni X, Bieri O, Schoenberg SO, Trattnig S, Zbyn S. In vivo sodium (23Na) imaging of the human kidneys at 7 T: preliminary results. Eur Radiol 2014;24(2):494-501.

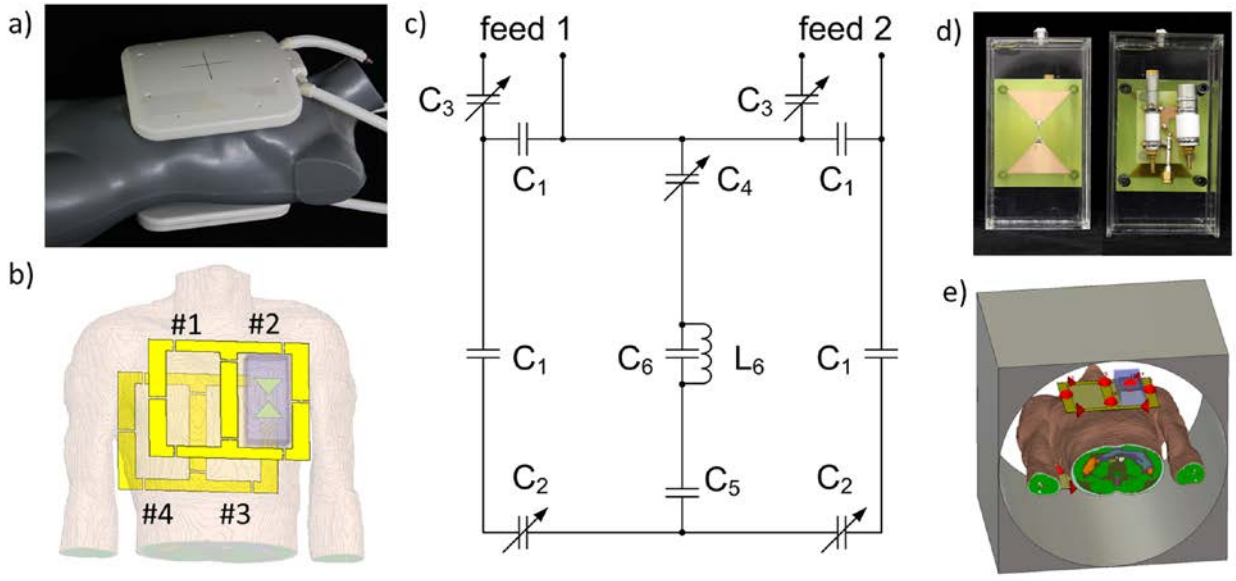

Figure 1:

Overview of the proposed $^{1}H/^{23}Na$ RF coil array tailored for cardiac ^{23}Na MR at 7.0 T. **a)** Anterior and posterior coil section of the proposed sodium RF coil array placed on a mannequin. **b)** Basic loop structure and element numbering of the sodium array shown in the simulation model. **c)** Circuit diagram of the anterior section of the sodium loop array. **d)** Picture photograph of the dipole element used for proton imaging, which was placed inside loop element two as illustrated in b). **e)** Simulation setup consisting of the sodium array, the dipole element and the voxel model Duke inside the bore given by the gradient shield.

a)

78.6 MHz	1	2	3	4	1H
1	-23.4	-20.8	-inf	-inf	-49.2
2		-18.5	-inf	-inf	-55.1
3			-17.2	-29.7	-inf
4				-15.3	-inf
1H					-0.2

b)

297 MHz	1	2	3	4	1H
1	-1.5	-34.1	-inf	-inf	-26.8
2		-1.4	-inf	-inf	-26.4
3			-1.2	-51.0	-inf
4				-1.1	-inf
1H					-26.2

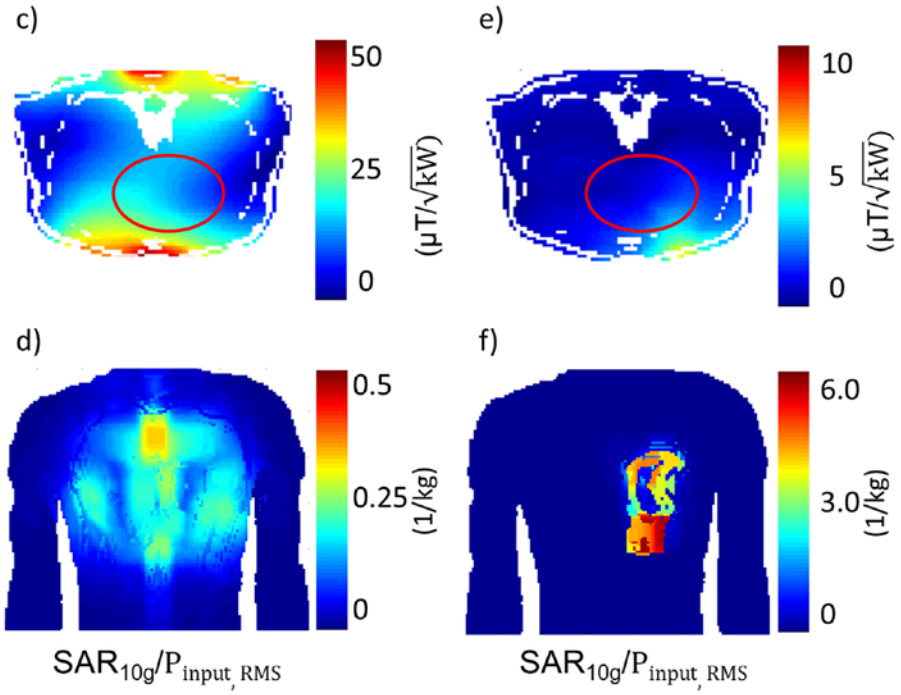

Figure 2:

Synopsis of the results derived from EMF simulations and measurements of the RF characteristics of the ^{23}Na/^{1}H setup. **a)** Scattering parameters measured on a subject to demonstrate the resonance behavior of the ^{23}Na/^{1}H setup at 78.6 MHz. **b)** Scattering parameters measured on a subject at 297 MHz. **c)** Transmission field simulation for the four channel ^{23}Na array using a circular polarized phase setting depicted in a transversal plane through the heart marked by the ROI shown in red. **d)** Maximum projection plot of the local SAR_{10g} distribution of the ^{23}Na array simulated for the human voxel model Duke based on the circular polarized phase setting. **e)** Transmission field simulation at 297 MHZ for the ^{1}H dipole element depicted in a transversal plane through the heart (ROI in red). **f)** Maximum projection plots of the local SAR_{10g} distribution of the ^{1}H dipole element simulated for the human voxel model Duke.

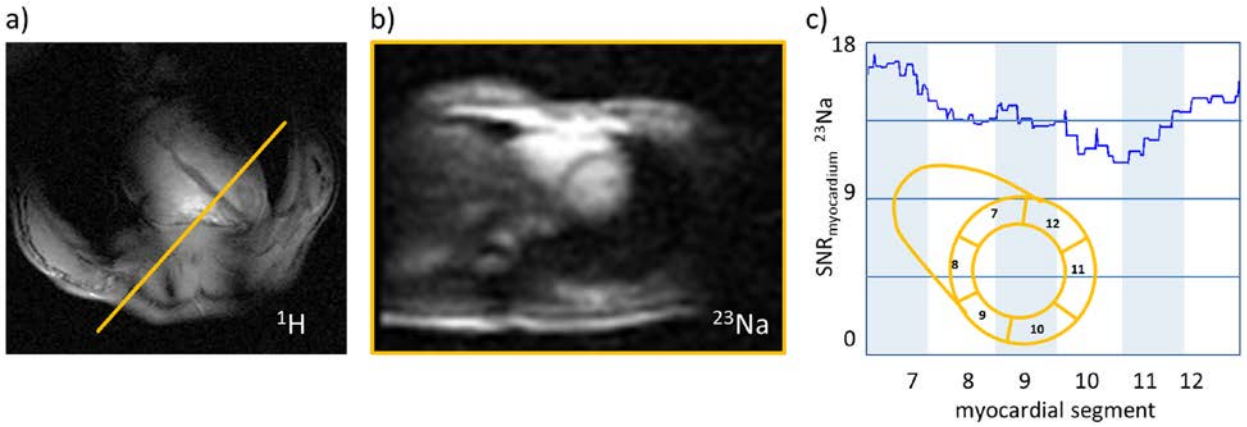

Figure 3:

a) ^{1}H four chamber view localizer of the heart derived from 2D CINE gradient echo imaging using the dipole element. This systolic view was used for planning the 3D slabs employed in ^{23}Na MRI, which were centered around a mid-ventricular short axis view marked by the orange line. **b)** ^{23}Na short axis view of the heart acquired with the four channel loop array at the mid-ventricular slice position indicated in the ^{1}H four chamber view shin in **a)**. A 3D gradient echo imaging protocol was applied for data acquisitions. **c)** SNR evaluation for the mid-ventricular short axis view shown in **b)** following a trajectory along the myocardial segments 7-12. To guide the eye, the standardized myocardial segment model proposed in (30) is illustrated in orange.

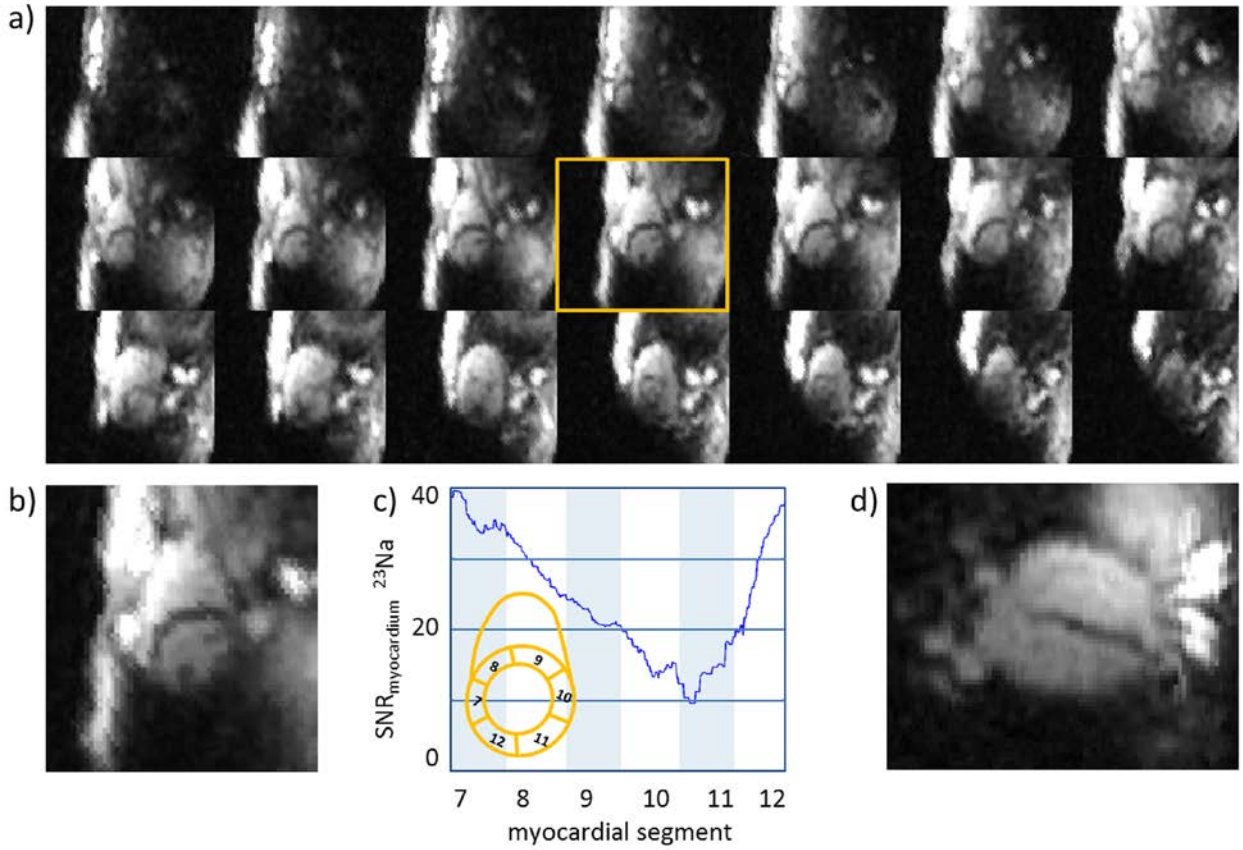

Figure 4:

Cardiac ^{23}Na images derived from ungated reconstruction of a 3D dataset which was acquired with a nominal isotropic spatial resolution of 6 mm using the 3D density-adapted radial acquisition protocol. Standard cardiac views were extracted using normal vectors from ^{1}H image positioning. **a)** A stack of short axis views covering the whole heart from the apex to the atrium. **b)** Mid-ventricular short axis view used for SNR evaluation. **c)** SNR evaluation for the mid-ventricular short axis view shown in b) following a trajectory along the myocardial segments 7-12. **d)** Four chamber view of the heart retrospectively reconstructed from the 3D whole heart coverage data set.

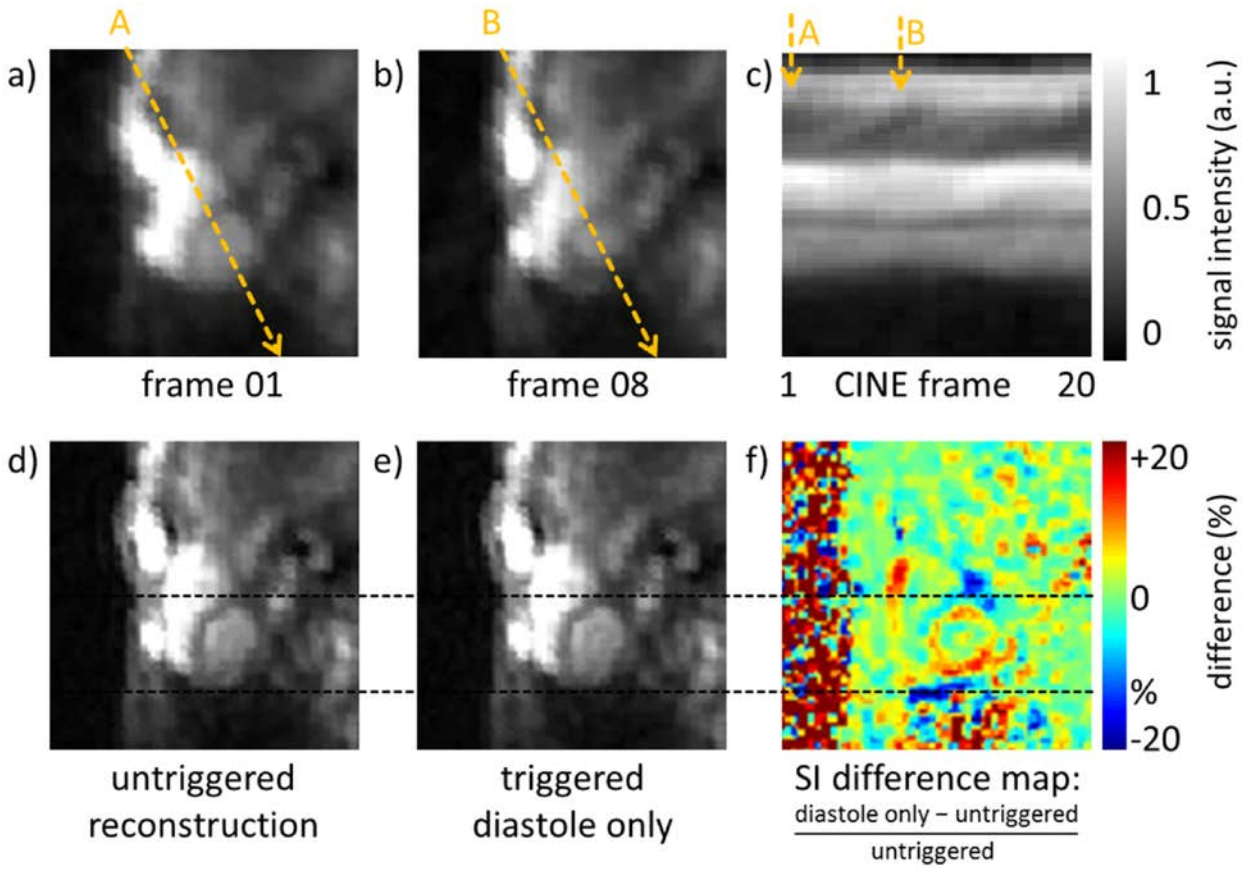

Figure 5:

Cardiac CINE images reconstructed from a 3D dataset with a nominal isotropic spatial resolution of 6 mm which was acquired with the 3D density-adapted radial protocol. Retrospective gating was applied during reconstruction using time increments of 0.05 s and time frames of 0.1 s. Short axis views were extracted using the normal vector from ^{1}H image positioning. **a)** Mid-ventricular short axis CINE frame in diastole. **b)** Mid-ventricular short axis CINE frame in systole. **c)** M-mode like, temporally resolved signal evolution extracted from the profile placed along the long axis of the heart, as depicted in a) and b), for all 20 frames of the CINE acquisition. The line shown in a) and b) are marked by the arrows A and B. **d)** Ungated reconstruction based on the complete dataset. **e)** Selective reconstruction of diastolic data acquired between 0.6 s and 1.2 s after recognition of the onset of the cardiac cycle using the acoustic cardiac triggering device. **f)** Difference map of images deduced from ungated and gated reconstruction which revealed a blood pool signal gain of +20% of the gated image. This behavior helped to enhance the delineation between blood and myocardium.